The International Journal of Advanced Manufacturing Technology (2024) 130:1735–1747
https://doi.org/10.1007/s00170-023-12738-7

ORIGINAL ARTICLE

Investigation of surface imperfection in freeform optics with high-order XY polynomial design

Sumit Kumar[1] · Wenbin Zhong[1] · Guoyu Yu[1] · Jufan Zhang[2] · Wenhan Zeng[1] · Xiangqian Jiang[1]

Received: 10 August 2023 / Accepted: 23 November 2023 / Published online: 13 December 2023

Abstract
Freeform surfaces find potential applications in optics but pose new challenges for manufacturing and functional testing. A basic description of such surfaces is observed in terms of surface spatial frequencies which have been altered as a result of evolution in the fabrication of optics. While mid-spatial-frequency (MSF) errors arising from manufacturing and metrology processes are well documented, our investigation reveals that such errors originate not only during these stages but also during the surface construction at the design phase, particularly for high-order XY polynomial optical surfaces. The presence of MSF errors can significantly affect the performance of high-performance optical systems across various applications. The study discussed in this paper focuses on the relationship between the resolution of the design dataset of freeform surfaces with high-order polynomials and the subsequent surface imperfections in the production of precision optics. The main contributions of this investigation are the identification of MSF errors at surface construction of the design phase and the control over the MSF errors in design dataset using the 2nd-order Gaussian filtration which will bridge the gap between freeform optics design and ultra-precision manufacturing.

Keywords Freeform optics · Mid-spatial frequency · Surface imperfection · Filtration · Data analysis

1 Introduction

The field of optics has served an essential role in the advancement of science and technology, with evidence of lens production dating back to the ancient Egyptians as early as 2000 BC [1]. Modern applications in numerous fields including astronomy, medicine, and telecommunications, to name a few, have benefited from the advancement of optics from flat, spherical, aspheric, and now to freeform optics. Today, we rely on optical systems and devices more than ever before. A substantial percentage of the population either uses mobile devices that are packed with miniaturized optical components or driving vehicles that have multiple displays, cameras, and optical sensors. On the other hand, conventional optics rely on heavy, bulky, and functionally constrained components which limits their use in some circumstances namely the optical properties such as transmittance and reflectance constraints. The production of conventional optics involves the fundamental principle of rubbing and involves abrasion mechanisms such as grinding and polishing [2]. Shape, surface texture, surface roughness, and subsurface damage are the quality criteria for the surface after the traditional manufacturing process. Recurring patterns remain observable when traditional procedures using different non-complex ways are used to generate the surfaces. These regular patterns are often referred to as MSF errors. Even when the amplitude of MSF content is just a few nanometres, such frequencies can result in significant degradation of the optical performance due to interference and diffraction within the light beam propagating through the system [3]. It is safe to assume that the irregularity is caused by low-order aberration like astigmatism. These errors can be modelled by optical design software. In diamond turning operations, we can predict the MSF to high-frequency ripples in the rotatory symmetrical optical element [4]. However, problems arise in generating freeform surfaces with higher order polynomials due to tedious huge

✉ Wenhan Zeng
Z.Wenhan@hud.ac.uk

[1] EPSRC Future Metrology Hub, Centre for Precision Technologies, School of Computing and Engineering, University of Huddersfield, Huddersfield HD1 3DH, UK

[2] Centre of Micro/Nano Manufacturing Technology (MNMT-Dublin), School of Mechanical and Materials Engineering, University College Dublin, Dublin 4, Ireland

data handling of complex mathematical functions. Freeform surfaces are those surfaces that lack an axis of rotational invariance or are axially imbalanced [5–7]. The freeform surface is now an emerging field in a wide range of optical systems. From a design standpoint, aspheric and off-axis design is analogous to freeform design in numerous ways.

In this research, surface imperfection in high-order XY polynomial freeform surface is investigated to mitigate the performance loss of the optics. The root cause of MSF errors is identified and surface imperfections caused by these MSF are eliminated by employing the 2nd order Gaussian filtration to the design surface dataset. A high-order XY polynomial of 10th order freeform surface is considered in this research to understand the issues related to the surface imperfections. The problems related to MSF errors affecting the quality of the optics are identified with three different approaches, i.e., spatial space, frequency domain, and periodicity of the surface features. The proposed data analysis method is effective in eliminating surface imperfection via controlling the MSF errors in the design dataset.

2 Background

When the freeform optical surface is designed using the high-order XY polynomial of 10th order and the dataset produced is of the non-uniform resolution then the fabrication results in complex MSF errors which are periodic features. To our best knowledge, the present investigation on surface imperfection of high-order XY polynomial of 10th order freeform surface at the design phase is conducted for the first time. Due to the lack of documented design work in this field, we attempt to clarify the MSF concepts using the fabrication-based literature. Most of the periodic vibrations or movements have a connection to controllable parameters in the manufacturing process [8]. Certain vibrations are constant throughout the complete process and are not related to the fabrication parameters [9]. MSF errors are separate from surface roughness and can emerge at spatial frequencies that range from 0.01 to 10s of mm^{-1} [10]. However, the spatial frequency range is specified in terms of surface aperture size, manufactured, and measured. The MSF error in an optical system has no fixed frequency limits, rather it depends on the manufacturing methods used to generate the optics through the location-specific or sub-aperture material removal process. The MSF errors are structural error types which emerge on the surface with various signatures (such as spiral, milled, and turned) resulting from various fabrication methods [11–14]. Such errors have a major influence on the optical performance, i.e., image quality and point spread function of the optical system [15, 16]. There are various precision manufacturing processes that are applied for correcting these periodic features after performing diamond turning on the optical components such as ion beam figuring [17], magnetorheological finishing [18], and computer-assisted polishing [19]. Additionally, in diamond turning, the toolpath management plays a critical role in the control of MSF errors. Also, typical toolpath generation based on the principle of automatic dynamics analysis of mechanical systems provides adequate control over the MSF errors in order to reduce the duration of post-diamond cutting operations for better functioning of the freeform optical surface [20].

The main reasons for surface imperfection in ultra-precision manufacturing of freeform optics have been identified and they are listed below for now,

- Design dataset with unequal resolutions in equal rows and columns.
- Misalignment of the optical element to the chuck, tool, or measuring sensor.
- Tooling errors on the optical surface.
- Thickness variations of the workpiece (optical component) and clamping mechanism.

3 Methodology

In this study, the design phase is categorized into two domains, i.e., design-to-function and design-to-manufacture. In the design-to-function domain, the surfaces, components, and systems are optically designed and possess functionalities. However, due to the complexity of the shape, size, coordinate resolution, and many more, these designs are non-manufacturable with existing technologies. On the other hand, optical designs can be readily translated into appropriate manufacturing data in the design-to-manufacture realm. The surface representation of the freeform optical surface is considered as high-order XY polynomial which is expressed in Equation (1),

$$Z = \sum_{i=1}^{m} \sum_{j=1}^{n} f(X^m Y^n) \tag{1}$$

where sagitta Z of the surface is the function of X and Y coordinates with m and n as order of the polynomial equation. Particularly, high-order XY polynomial of degree 10 is considered under this investigation. The degree of a polynomial is the highest power of X, Y in its expression. The very first polynomials used for low-order freeform surfaces were XY-polynomials [21]. The XY polynomials surfaces descriptors for freeform optical surfaces are also found to be beneficial in terms of simplicity to model a surface. Apart from the easy handling, the XY polynomials descriptors are also found in numerous commercial optical design software [22]. There is a lot of potential to control the aberration with a low slope variation-based freeform surface

by using the XY polynomials descriptors [23]. Since this study often involves imaging applications using freeform optical surfaces, the XY polynomials descriptors for mild freeform optics have been taken into consideration in our design approach. In order to prevent machining errors while generating toolpaths, the spacing between the design coordinates of a non-symmetrical surface's point cloud should be as small as achievable. The data conversion algorithm [24] is applied to compile the data of on-machine surface measurement (OMSM) into surface data file (SDF) format for further analysis by MountainsMap and SurfStand surface analysis software. Similarly, the design dataset of lower resolution is converted to a higher resolution for bridging the gap between the design-to-manufacture of such complex surfaces. The data conversion includes three steps as follow: (i) Delaunay triangulation was performed on raw data ($D_{(Raw)}$) points in the XY plane; (ii) the triangle that encloses a given interpolated point is identified; and (iii) linear interpolation was performed within the triangle to determine the Z value of the point.

Surface imperfection problems in precision optical components lead to a reduction in the product life cycle and an enormous increase in manufacturing costs due to repeated iterations and compensation cycles. To address these challenges, a data analysis framework is developed for the design surface datasets as shown in Fig. 1. Initially, the raw design surface having the unequal resolution in horizontal and vertical domain of dataset is used to generate the toolpath. Due to the non-uniform dataset, the surface produced based on this dataset contains additional errors apart from fabrication, alignment, and metrological errors that result in improper functionalities in

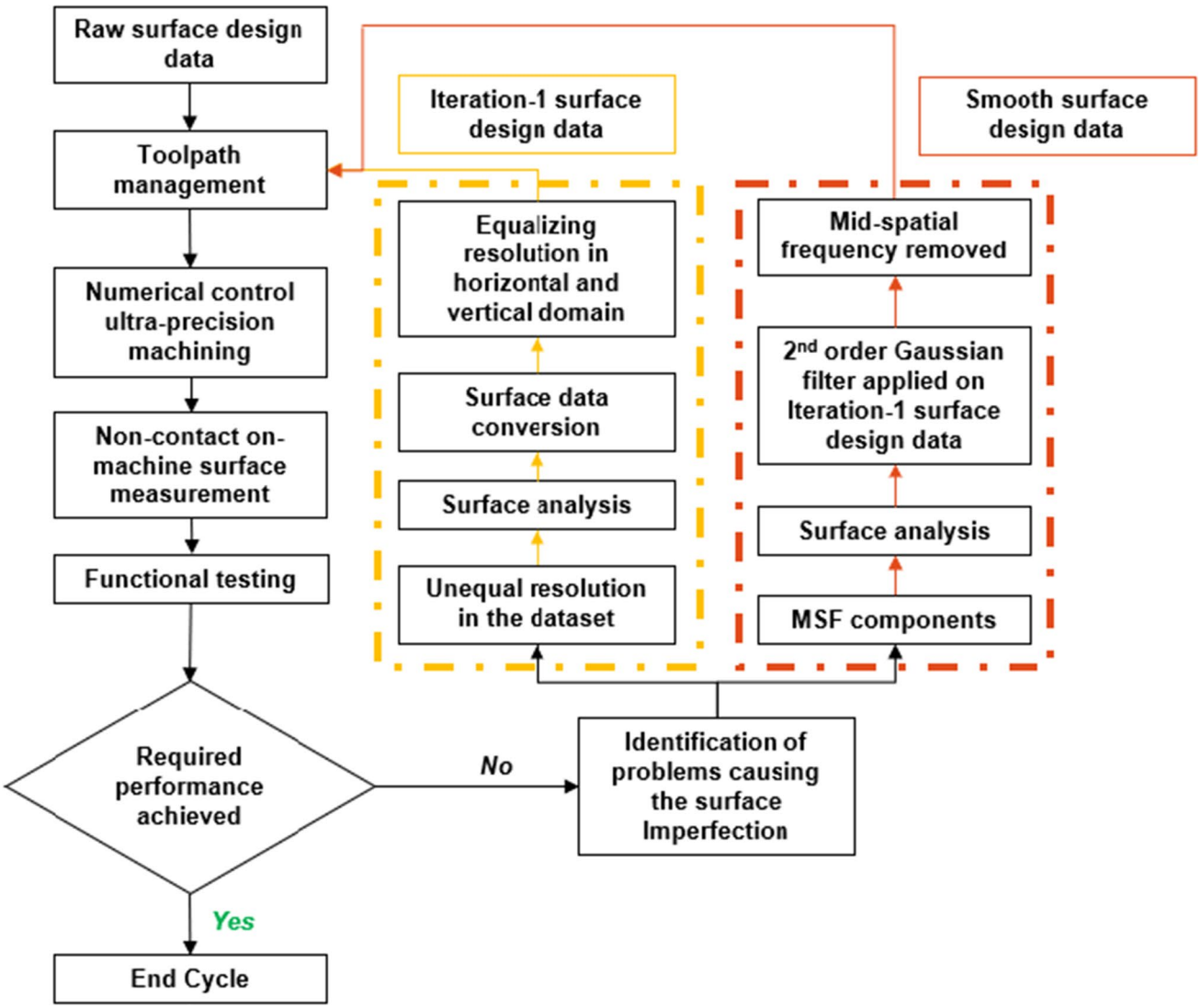

Fig. 1 Proposed surface data analysis framework to study surface imperfection in high-order XY polynomial freeform surfaces

high-order XY polynomial freeform surface. Therefore, the next prominent task is to convert the dataset into equal resolution dataset. This data conversion is performed in three different stages. First, the mesh grid of the surface with unequal resolution in horizontal and vertical direction is projected on the XY plane. Second, the surface is equally divided in X and Y directions and rows and columns are determined based on the surface dimension, i.e., clear aperture size is considered in our investigation. Third, each coordinate is matched with mesh grid of the surface in 3D space. Further, the Iteration-1 design dataset ($D_{(Iteration\text{-}1)}$) is used for toolpath management in ultra-precision manufacturing. Here, due to highly dense huge design dataset, regular patterns or MSF error of large magnitude are introduced. The same process of fabrication is followed to generate the freeform surface with high resolution data, i.e., 10 µm × 10 µm in rows and columns. With the residue MSF in dataset, the surface generated contains surface imperfection distributed over the fabricated freeform surface that results in degradation of optical performance. To minimize these MSF in $D_{(Iteration\text{-}1)}$ design dataset, 2^{nd} order Gaussian filtration is applied. The magnitude of the MSF contributing to the surface imperfection is controlled under 10 nm over the whole surface. Similarly, the defect-free toolpath management is employed to generate the freeform optical surface through ultra-precision diamond cutting.

The flowchart is explained with the help of three cases for design, manufacturing and controlling the surface imperfection through MSF errors as follows:

- If the design dataset contains rows and columns of equal and ultra-precision manufacturing required resolution, then the freeform optics can be directly produced through step 1.
- If the required optical performance is not achieved and the design dataset contains rows and columns of unequal and ultra-precision manufacturing required resolution, then the design dataset must be converted to equal-resolution spaced rows and columns as part of the design-to-manufacture approach. Further, the toolpath is generated based on the $D_{(Iteration\text{-}1)}$ which is used for producing freeform optics with high-order XY polynomial of 10th order.
- If the required optical performance is still not achieved with the above step, then the $D_{(Iteration\text{-}1)}$ design dataset is further converted to the $D_{(Smooth)}$ design dataset by implementing 2^{nd} order Gaussian filtration. Manufacturing of freeform optics of high-order XY polynomial of 10th order with toolpath based on the $D_{(Smooth)}$ design dataset controls surface imperfections.

4 Identification of MSF from the design dataset

A surface is a vector or raster dataset that contains an attribute value for every locale throughout its extent. Spatial interpolation techniques are based on Tobler's first rule of geography which states that "everything is related to everything else, but near things are more related than distant things" [25]. An in-depth knowledge of huge-data management is essential to eliminate the fundamental root cause of MSF errors in freeform optical surfaces through ultra-precision manufacturing. For this, two influencing factors need to be defined, the first is interpolation and curve fitting, and the second is filtration [26]. Interpolation is to connect discrete data points so that one can get reasonable estimates of data points between the given points. Whereas curve fitting is to find a curve that could best indicate the trend of a given set of data. B-spline and non-uniform rational B-spline (NURBS) are the preferable approximation forms from the perspective of freeform design and manufacturing. Approximations are fitted to a set of discrete data to obtain the functional representation of freeform surfaces.

As shown in Fig. 2, the designed freeform optical surface is presented with the sagitta with a peak-to-valley (Pt) in millimeter distributed across the 140.4 mm × 105 mm area. The freeform surface is described by high-order XY polynomial. Considering the design based on the manufacturing and metrology-oriented scheme, the functional aperture is extracted for further processes. Depending upon the type of application, the functional area (clear aperture in physical optics) from the whole of the designed surface is extracted.

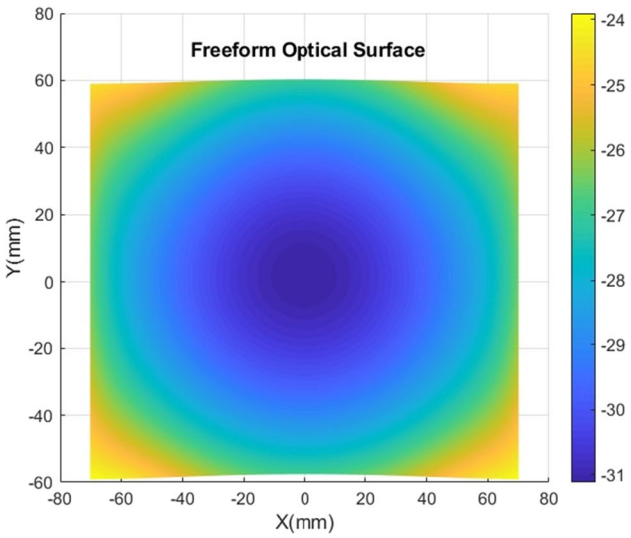

Fig. 2 Surface map of a freeform optical surface described by high-order XY polynomial

In this research, the dimension of the functional surface is 106 mm × 53 mm. Three different analyses at design phase for avoiding MSF errors in design-to-manufacture approach for high-order XY polynomial optical surface are performed. The surface analysis is carried out in the following steps: (i) distribution of regular features in terms of horizontal distance and magnitude, (ii) power spectral density (PSD), and (iii) feature/texture orientation.

4.1 Identification of MSF of design dataset in spatial space

According to ISO 3247 standard [27], it specifies that the primary profile should not contain the nominal form of the test specimen. Before doing any further metrological operations, the form must be removed. Due to the presence of non-planar form in the $D_{(Raw)}$ design dataset, the operation of form removal is performed. And for the form as just a line segment or plane, the levelling is performed. For surface analysis of $D_{(Raw)}$, the 2D profile is extracted with oblique scan as shown in Fig. 3. Typically, the average magnitude of the features on the 2D profile is observed as 21.102 nm of five different features with the regular intervals. These regular features are present on the profile at the average horizontal distance of selected features that are observed as 1.077 mm over the scan of 45 mm. Such spacing is not sufficient in generating precise toolpath for ultra-precision manufacturing of freeform surface described with high-order XY polynomial. Therefore, the resolution of the design dataset is converted into equal spacing in MATLAB as presented in the previous Section.

The same procedure is followed in extracting the profile from the higher resolution design dataset $D_{(Iteration-1)}$, as shown in Fig. 4. The $D_{(Iteration-1)}$ design dataset is obtained by using data conversion technique for equalizing the resolution in X and Y coordinates of dataset as discussed in previous section. Due to registration issues, the profile from $D_{(Iteration-1)}$ design dataset is extracted within the closest zone as compared from the $D_{(Raw)}$ profile extraction. The features roughly at regular intervals are present in the extracted 2D profile. Average horizontal distance for the five selected features on the extracted 2D profile of $D_{(Iteration-1)}$ design dataset is 0.38264 mm. The average magnitude of selected features over the 2D profile of $D_{(Iteration-1)}$ design dataset is 29.708 nm.

Filtration on $D_{(Iteration-1)}$ design dataset with 2nd order robust Gaussian Filter [28, 29] is performed to obtain the $D_{(smooth)}$ design dataset. The 2D profile is extracted from $D_{(Smooth)}$ design dataset which contains similar features with long horizontal distance and shorter magnitude as shown in Fig. 5. The average height difference of the selected five peaks and valleys is 4.9989 nm and the average wavelength of the five selected features is 2.4088 mm in $D_{(Smooth)}$ design dataset.

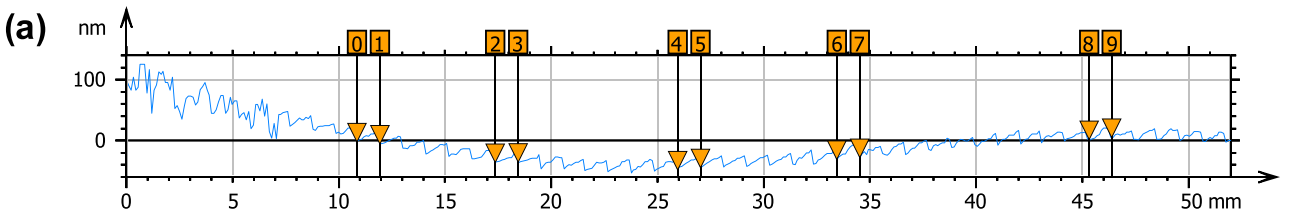

Parameters	Unit	0-1	2-3	4-5	6-7	8-9
Horizontal distance	mm	1.084	1.079	1.076	1.086	1.060
Oblique distance	mm	1.084	1.079	1.076	1.086	1.060
Slope	nm/mm	-3.461	0.6133	3.275	2.754	3.196
Mean height	nm	5.951	-29.67	-36.75	-17.55	11.18

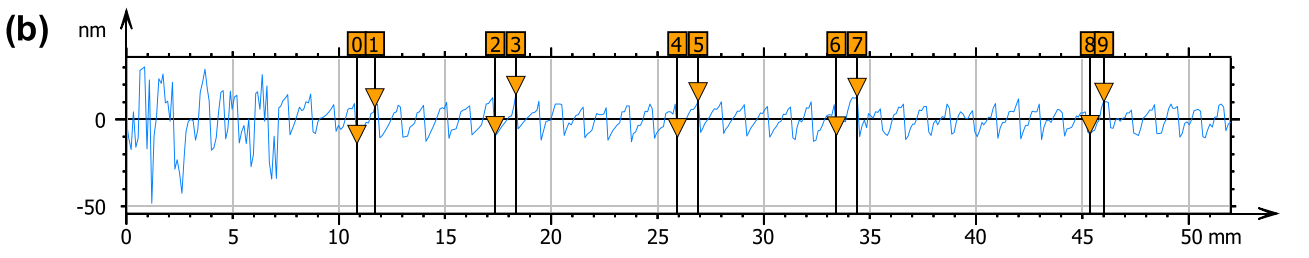

Parameters	Unit	0-1	2-3	4-5	6-7	8-9
Height difference	nm	21.05	23.07	20.73	22.10	18.56

Fig. 3 Profile scan from $D_{(Raw)}$ for evaluation of (a) horizontal distance and (b) amplitude

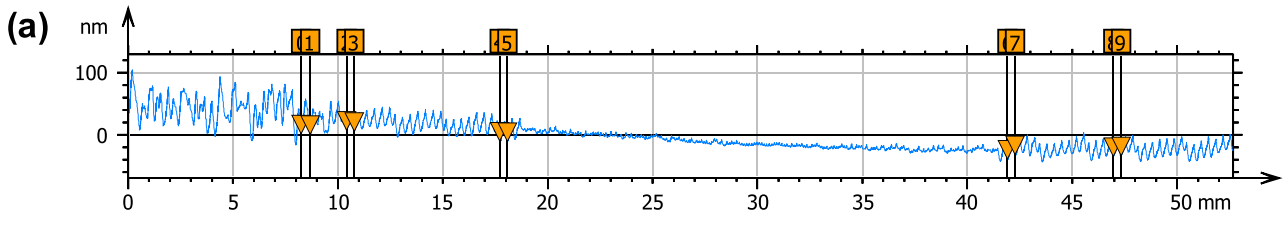

Parameters	Unit	0-1	2-3	4-5	6-7	8-9
Horizontal distance	mm	0.4320	0.3687	0.3699	0.3670	0.3756
Oblique distance	mm	0.4320	0.3687	0.3699	0.3670	0.3756
Slope	nm/mm	-1.588	-5.191	-2.066	19.14	3.071
Mean height	nm	30.67	19.62	1.989	-24.76	-24.19

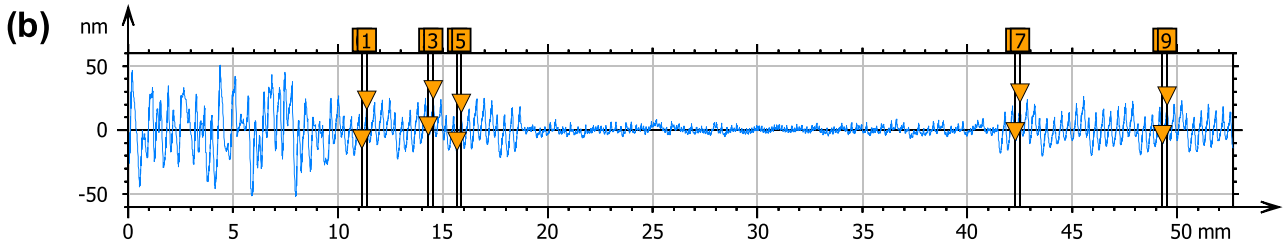

Parameters	Unit	0-1	2-3	4-5	6-7	8-9
Height difference	nm	30.35	28.21	29.61	30.22	30.15

Fig. 4 Profile scan from $D_{(Iteration\text{-}1)}$ for evaluation of (a) horizontal distance and (b) amplitude

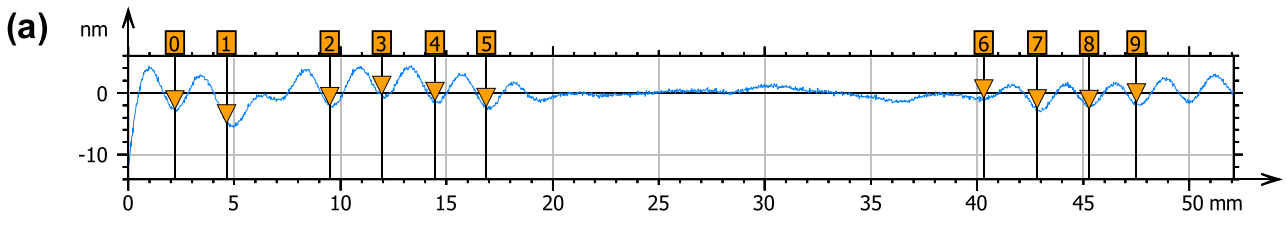

Parameters	Unit	0-1	2-3	4-5	6-7	8-9
Horizontal distance	mm	2.434	2.450	2.411	2.520	2.229
Oblique distance	mm	2.434	2.450	2.411	2.520	2.229
Angle	°	-5.333e-05	4.219e-05	-2.338e-05	-3.63e-05	2.701e-05
Mean height	nm	-0.2703	1.257	0.5045	-0.2206	-0.2433

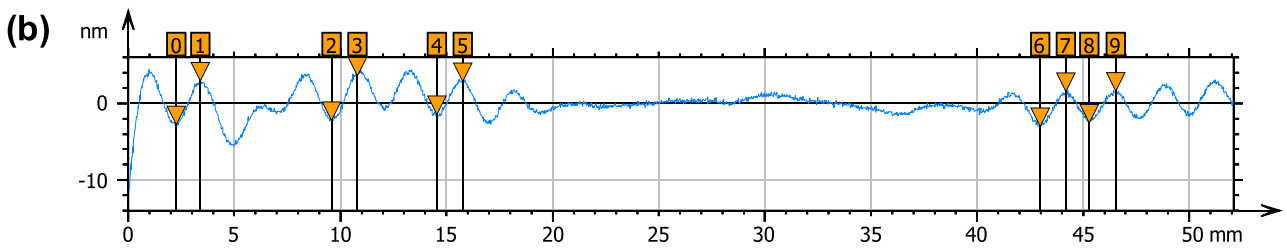

Parameters	Unit	0-1	2-3	4-5	6-7	8-9
Height difference	nm	5.714	6.261	4.297	4.564	4.156

Fig. 5 Profile scan from $D_{(Smooth)}$ for evaluation of (a) horizontal distance and (b) amplitude

4.2 Identification of MSF of design dataset in frequency domain

Power spectral density (PSD) graphs can be used to display and explain MSF errors. Here, average PSD plots, in a nutshell, explain how a surface's amplitude relates to frequency. Fast Fourier transformations (FFT) of the optical surface sampling, on which PSD plots are based, enable examination into the prominent frequencies of errors over the band of interest. Figure 6 shows a graph that describes the behaviour of the amplitude of the MSF error peaks from (a) $D_{(Raw)}$, (b) $D_{(Iteration\text{-}1)}$, and (c) $D_{(Smooth)}$ with respect to its spatial frequency. The identified peaks of $D_{(Raw)}$ are from (i) to (xvi), of $D_{(Iteration\text{-}1)}$ are (x) to (xvi), and of $D_{(Smooth)}$ are from (xvii) to (xxviii) which are clearly visible and can be well distinguished from the "data transfer, orientation, and control of resolution". The maximum amplitude of the frequency peak from the $D_{(Raw)}$ design dataset is found as peak-(v) 214.1 nm, for $D_{(Iteration\text{-}1)}$ design dataset is peak-(x) 132.5 nm and for $D_{(Smooth)}$ design dataset is peak-(xvii) 12.03 nm. The MSF errors in terms of amplitude are identified using PSD and are found to be in good relationship with the magnitude of the features extracted from 2D profiles as shown in Figs. 3, 4, and 5. Intensity of peak-(ii) in $D_{(Raw)}$, peak-(xiv) in $D_{(Iteration\text{-}1)}$, and peak-(xxvi) in $D_{(Smooth)}$ observed the magnitude of 20.35 nm, 36.09 nm and 7.935 nm. Peaks with higher amplitude are precisely controlled under 20 nm over the whole surface from the initial to the final design dataset with filtration.

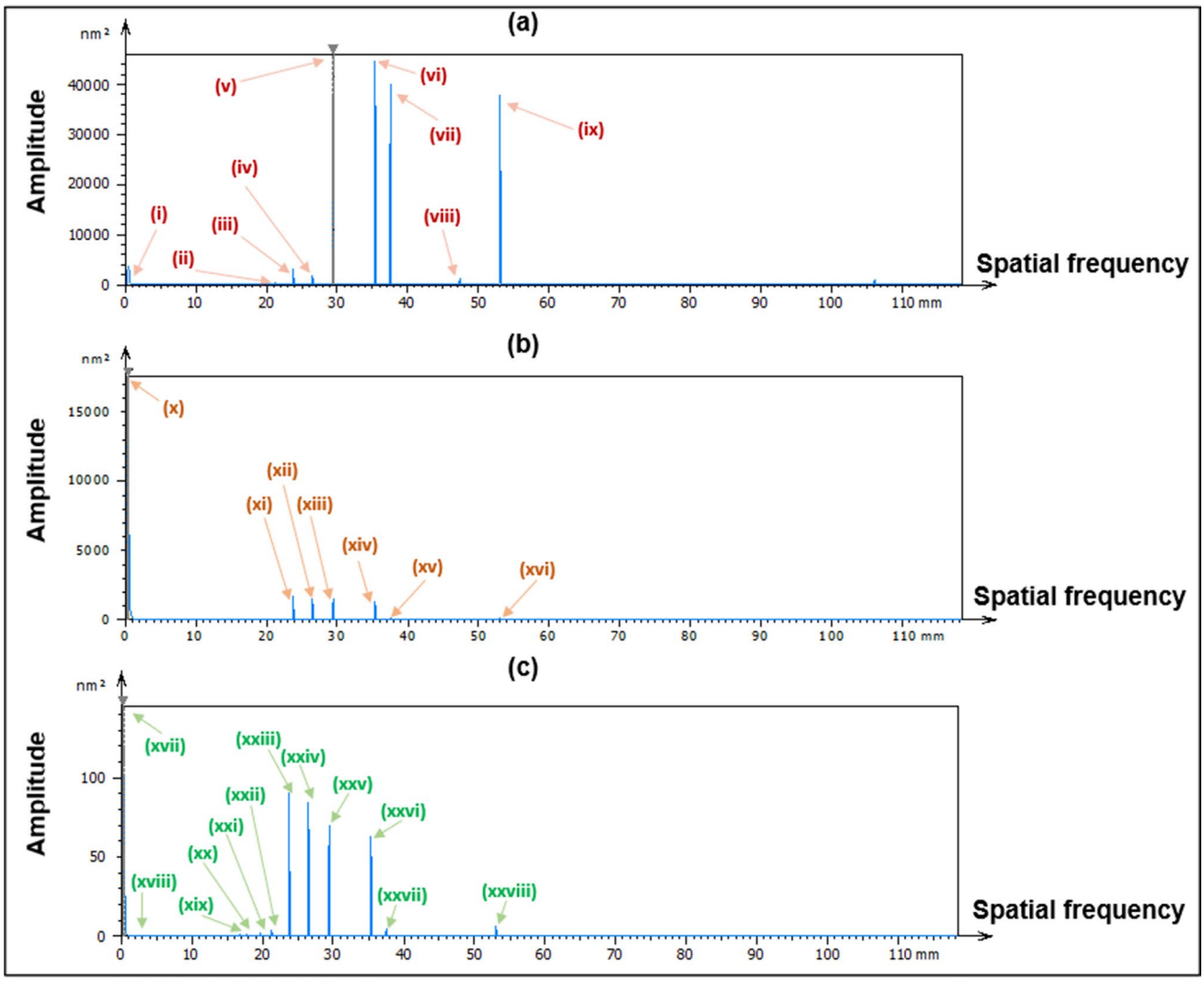

Fig. 6 Averaged PSD plots of the datasets of (a) $D_{(Raw)}$, (b) $D_{(Iteration\text{-}1)}$, and (c) $D_{(Smooth)}$

4.3 Identification of anisotropic phenomena from design dataset

Figure 7 shows the periodicity difference of anisotropic surface (surface with regular features) and isotropous surface. For isotropic surfaces, the characteristics of spatial frequency remain the same at every direction as shown in Fig. 6(a) and (c). The main root cause of surface imperfections in design-to-manufacturing of freeform optics are the coordinate distribution characteristics of the multiple design datasets and the influence of resolution on the surface during surface data conversions. The design dataset describes the isotropic and anisotropic behaviour during the design phase and further lays the imprint on manufacturing. Materials like steel, copper, beryllium, aluminium, and alloys typically have isotropic properties. Whereas the carbon fibre, graphite, and many other materials have anisotropic characteristics. For the current study, the periodicity transition is analysed and observed at design phase of the different design datasets. The evaluation of the difference between the original and final freeform optical surfaces is carried out separately from the analysis. The cause for the final errors due to resolution of datasets is also compared with the close-to-perfect design dataset. Figure 8 illustrates the difference between the raw design surface ($D_{(Raw)}$) and the smooth design surface ($D_{(Smooth)}$)

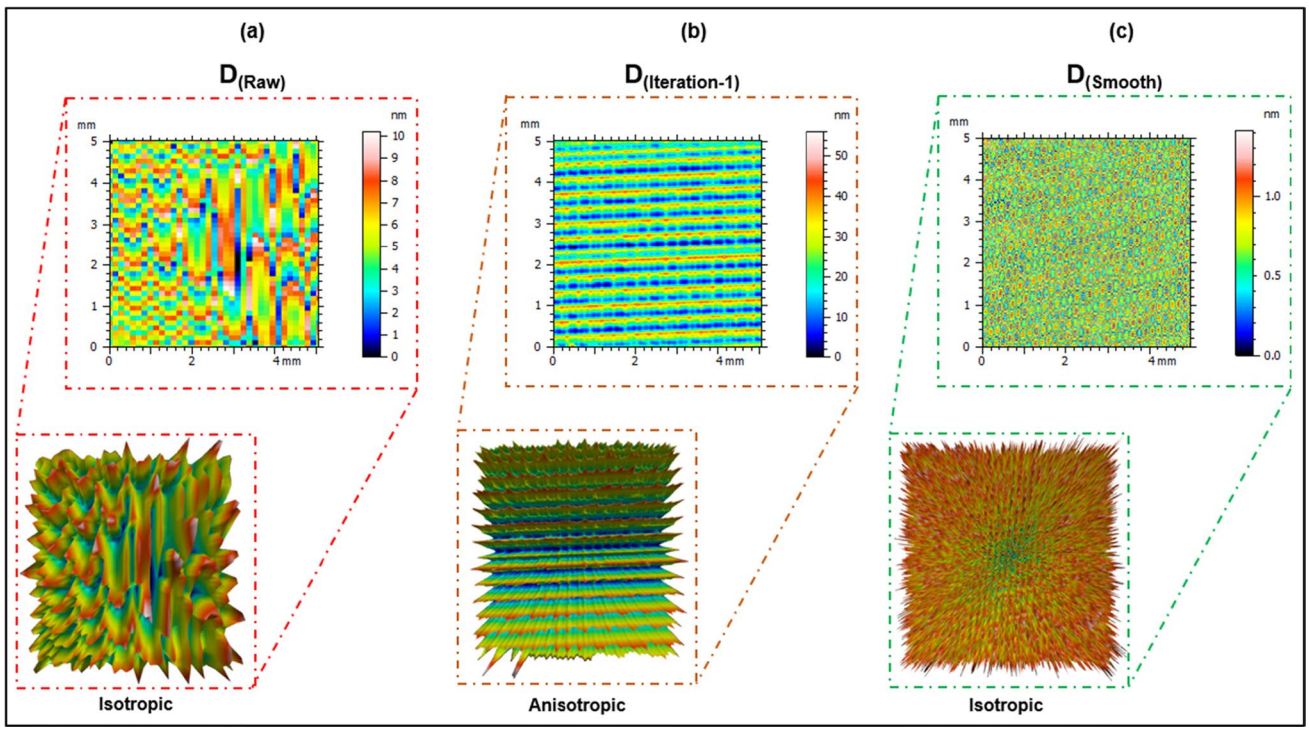

Fig. 7 Periodicity of different surface, (a) $D_{(Raw)}$, (b) $D_{(Iteration-1)}$, and (c) $D_{(Smooth)}$

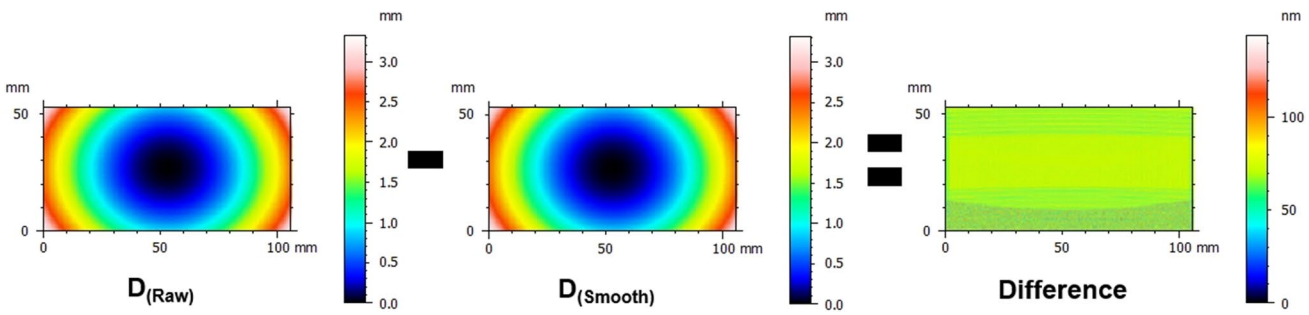

Fig. 8 Difference between the raw design surface ($D_{(Raw)}$) and smooth design surface ($D_{(Smooth)}$) with MSF removed at the design phase of freeform optics

while designing a freeform optical surface after MSF was eliminated.

5 Discussion

Due to the non-symmetrical nature of freeform surface, the features are present in irregular pattern for high-order XY polynomial. This makes the surface analysis process more sophisticated in terms of orientation selection and defining the clear aperture for analysis. It is clearly observed from the profiles of Figs. 3, 4, and 5 that with equalizing the resolution between the rows and columns in 2D increases the frequency of the points over the whole selected surface. Also, the reduction in spacing between a set of points describing the X and Y coordinate of a surface is found to be the cause for the MSF error and further to surface imperfection. In toolpath generation for ultra-precise freeform optical surfaces such uncontrolled splines have a tremendous effect on the optical performance of the surface after the diamond cutting operation. However, as identification of the fundamental cause at the earlier design phase of development minimize the quantity of errors and reducing the manufacturing cycle time and cost of the production. Therefore, this research is expanded in order to understand the contents of the current surface analysis better than with a traditional spectrum analysis. PSD study as shown in Fig. 6 provides the plots for all direction analysis to understand the magnitude of each wavelength from the frequency spectrum. The design datasets are used to categorize the MSF characteristics, and it is found that the wavelength magnitude is of nanometric range. As per spatial frequency, the figure errors are eliminated by removing the form from the surface and high-spatial frequencies, i.e., finish or roughness are not considered due to availability of low-density design dataset. The analysis is performed only on the design coordinates, i.e., no physical entities. In this study, only peaks lower than 100 nm are classified to have surface imperfections in the following phases.

As working in nanometric level, the spatial frequencies contributions from all the directions are analyzed in terms of texture isotropy. Therefore, the distribution of the features on the surfaces is generated using the ISO 25178 Standard [30]. Due to huge-data handling load on software and system, a small rectangular patch of dimension 5 × 5 mm is considered for the analysis of features. In order to develop deep knowledge of feature orientation, this study analyses texture isotropy and texture direction. The three peaks with the largest values are identified. The secondary peaks which are below 5° of an already detected peak are not considered into study. The first direction is equal to the ISO 25178 Standard value (with the reference angle at 0°). It is observed from Fig. 7(b) that the anisotropic distribution of coordinates is causing the MSF errors and further result in surface imperfection on performing fabrication operation with toolpath generated based on the surface of $D_{(Iteration\text{-}1)}$ design dataset. An additional texture direction analysis is carried out on the $D_{(Iteration\text{-}1)}$ design dataset due to inadequate texture isotropy percentage, that is, less than 30% on the selected 5 × 5 mm patch. Fig. 9 shows the distribution of the texture directions with the highest peak with precisely close to 0°, whereas the second and third highest peak has the texture direction of 90° and 7.48°.

The localized surface imperfection deteriorates the essential optical performance and optical quality of the optical

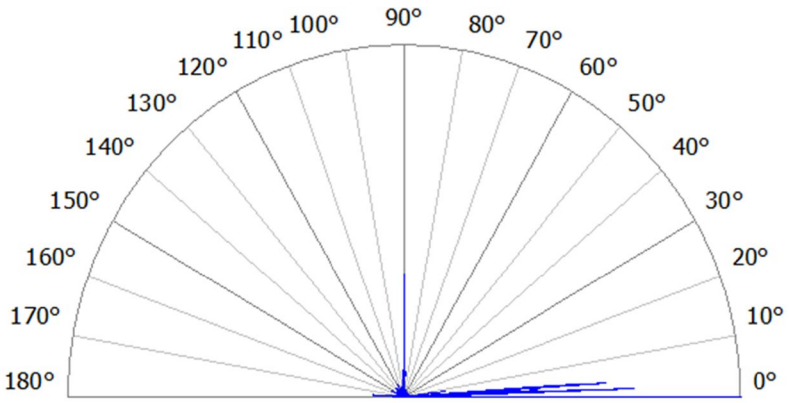

Parameters	Value	Unit
First direction	0.01355	°
Second direction	90.00	°
Third direction	7.480	°

Fig. 9 Texture direction of a selected 5 × 5 mm patch on $D_{(Iteration\text{-}1)}$ design dataset

component which can be identified visibly and according to the size [31]. On generating the toolpath based on $D_{(Iteration\text{-}1)}$ design dataset, the MSF features majorly contribute to the surface imperfection of the freeform optical surface as shown in Fig. 10(a). After the fabrication through ultra-precision single-point diamond turning (SPDT) the defects on the surface are quantified by observing changes in reflectivity at multiple zones of the freeform surface. These artefacts are observed in the region where the coefficient of high-order XY polynomial is high as compared with the coordinates in neighbouring zones. Control over the points functioned together to generate the toolpath which was then used by NURBs to generate surface. As a result, these types of non-uniform features with unpredictable direction adds complexity to the ultra-precision manufacturing processes and adds critical contribution in the MSF errors on surface. It is illustrated with the help of Fig. 7 that the $D_{(Raw)}$ design dataset behaves as isotropous surface making it functional but not manufacturable due to low-resolution dataset coordinates, i.e., 140.4 µm for rows and 105.1 µm. The development of toolpath and fabrication with such dataset may invite the figure error, i.e., form error that can significantly alter the required optical performance. Therefore, the two main strategies such as design-to-function and design-to-manufacture are simultaneously considered in ultra-precision freeform manufacturing. It is observed from Fig. 7(b) that the amplitude of the regular features increases and wavelength reduces. This may be causing uncontrolled orientation on the repeated features and further making the periodicity Anisotropic. On conducting the texture isotropy analysis, it is found that the isotropy reaches below 30% for test area. Therefore, the contribution of the texture's direction is analysed and found that the major peaks have 0.01355°, 90°, and 7.480° of texture direction. The uncontrollable direction of the nano-level peaks is also contributing towards the MSF followed by surface imperfections. So, there is a need to convert the anisotropic surface to isotropous surface for defect-free and smooth fabrication. As schematically shown in Fig. 8, the MSF contributes upto 40% of the overall surface which makes this component unusable. These MSF errors are balanced upto a required level of precision by implementing the 2nd order robust Gaussian filter on the $D_{(Raw)}$ design dataset because of the freeform nature of surface. These changes make the surface smooth with under 20 nm precision over the whole surface that provides sufficient space for controlling the z-value enclosed in the triangle for generating the toolpath for complex high-order polynomial surfaces. Figure 10(b) shows the fabricated surface with high reflectance after smoothening the design dataset with 2nd order robust Gaussian filter and also provides the clear illustration of the implementation of filtration at the design phase to limit the surface imperfection caused by the MSF. This novel ultra-precision manufacturing technique acts as the solid bridge between the gap of design and manufacturing.

OMSM with confocal probe is used to measure the freeform optical surfaces after machining with the developed toolpath based on the $D_{(Iteration\text{-}1)}$ and $D_{(smooth)}$ design datasets. Figure 11 shows the results of freeform machining before smoothing with toolpath $D_{(Iteration\text{-}1)}$ design dataset and freeform machining after applying the 2nd order Gaussian filtration to $D_{(Iteration\text{-}1)}$ design dataset. The result from measured profiles contains MSF errors contributed by other sources than that the design dataset such as machining and metrology. Due to unfiltered data, it is clearly seen that profile data has high frequency speckles. These speckles are

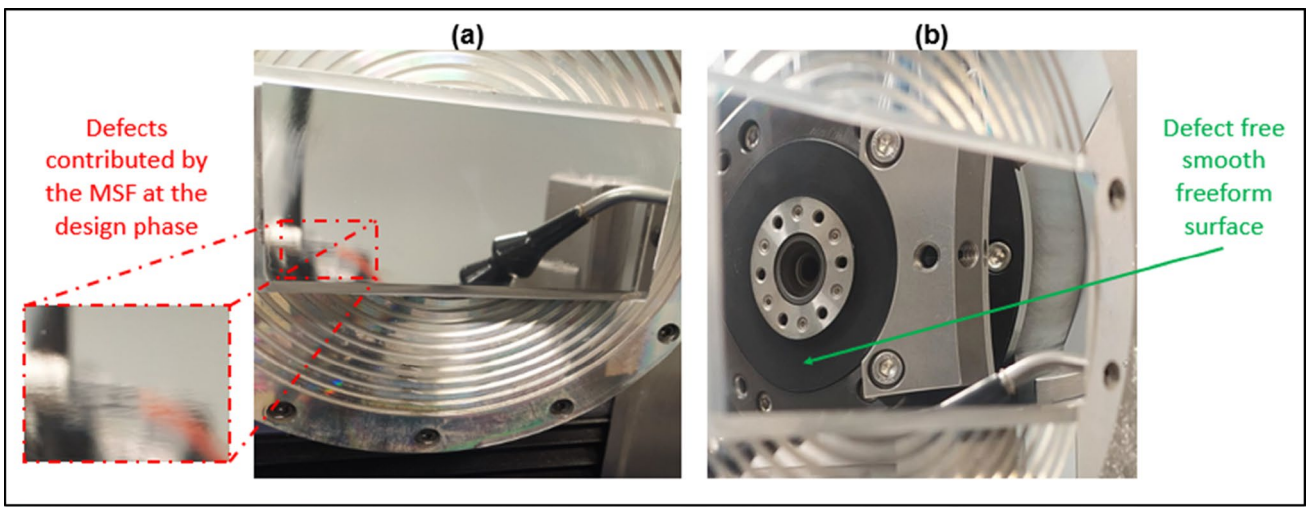

Fig. 10 Freeform optical surface fabricated using the ultra-precision single-point diamond turning on aluminium alloy with toolpath generated based on (a) $D_{(Iteration\text{-}1)}$ design dataset and (b) $D_{(Smooth)}$ design dataset

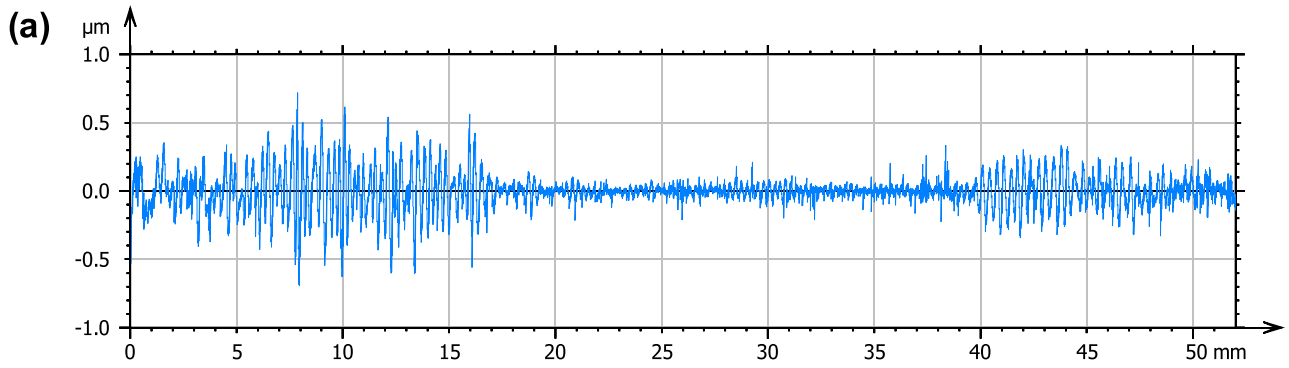

Parameters	Value	Unit
Pt	1.412	µm
Z-scale	2.000	µm

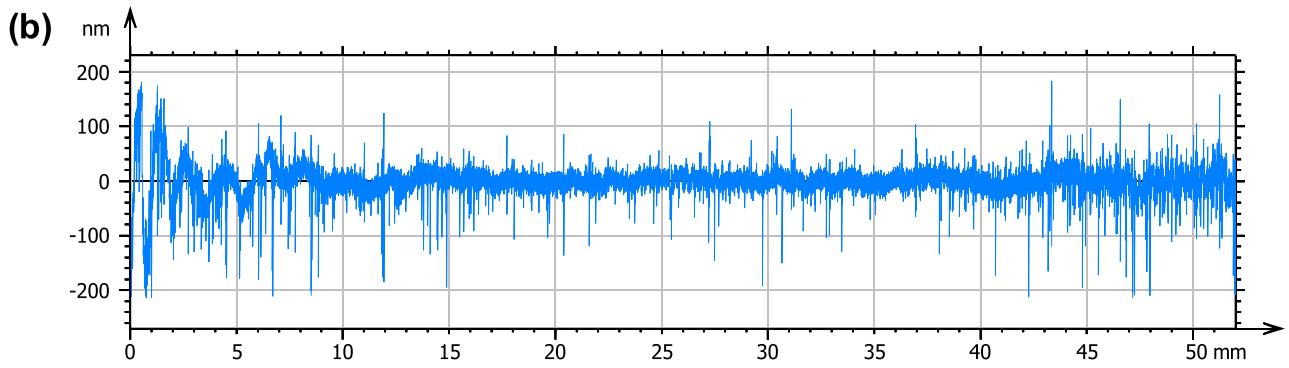

Parameters	Value	Unit
Pt	396.1	nm
Z-scale	500.0	nm

Fig. 11 Profiles scanned using on-machine surface measurement (OMSM) with a confocal probe on the freeform machined surface with toolpath generated based on (a) $D_{(Iteration\text{-}1)}$ design dataset and (b) $D_{(Smooth)}$ design dataset

caused by machining system dynamics and high measurement noise during the OMSM. The profile extraction was performed at the selected spot after the data analysis from Fig. 8 and the machined surfaces shown in the Fig. 10(a). The measured profile data is levelled, and the 10° of form is removed that removes the form of the freeform surface. The peak-to-valley (Pt) values of the manufactured surface with toolpath based on $D_{(Iteration\text{-}1)}$ and $D_{(Smooth)}$ was improved from 1.412 µm to 0.3961 µm.

6 Conclusions

Under this investigation, a root cause for the surface imperfection in high-order XY polynomial freeform surface manufactured through ultra-precision SPDT is identified. The major contributions of this research are (a) identification of the MSF error at the surface construction of the design phase and (b) proposed method to solve the surface imperfection problem such as the control over the MSF errors in design dataset using 2nd order Gaussian filtration. To our best knowledge, for the first-time, surface filtration is employed in developing ultra-high precision freeform optics to minimize the effects of surface imperfection.

The identification of MSF errors in the design datasets were performed in three stages, i.e., spatial domain, frequency domain, and anisotropic phenomenon of the surface features. In spatial domain, observations showed that the average magnitude of selected features over the 2D profiles of $D_{(raw)}$ is 21.102 nm, $D_{(Iteration\text{-}1)}$ is 29.708 nm, and $D_{(Smooth)}$ is 4.9989 nm.

The observations made in frequency domain of design datasets showed the maximum amplitude of the frequency peaks from $D_{(raw)}$ was 214.1 nm, $D_{(Iteration\text{-}1)}$ is 132.5 nm, and $D_{(Smooth)}$ is 12.03 nm. The peaks with higher amplitude were

precisely controlled to under 20 nm over the whole surface $D_{(Smooth)}$ with the 2nd order Gaussian filtration.

In isotropy analysis, the texture isotropy and texture direction were studied in order to acquire a deep understanding of the orientation of features. Due to inadequate texture isotropy percentage, i.e., less than 30% observed in $D_{(Iteration-1)}$ design dataset, an additional texture direction analysis was performed.

Based on the surface data analysis and proposed method to solve the issues of surface imperfection, the toolpaths were generated for the ultra-precision manufacturing of the freeform optics. Peak-to-valley (Pt) values of the produced surface were improved from 1.412 µm to 0.3961 µm with the toolpath generated based on $D_{(Iteration-1)}$ and $D_{(Smooth)}$.

Our initial research is a substantial contribution in filling the gap between design-to-manufacture of complexed high-order XY polynomial freeform optical surfaces. This novel approach finds potential benefits in the general data flow from design to fabrication applications of state-of-art modern optics and advanced optical system development. Also, the proposed method has potential in reducing the manufacturing iteration cycles for error compensation and machining time in ultra-precision SPDT. The optical designer needs to compensate for numerous manufacturing errors in addition to design aberrations. If not specifically minimised, the transfer of the design dataset to toolpath management in particular can have a disastrous impact on optical performance, especially for large aperture optics and large optical systems. Future work will focus on building closed-loop complexed modern optical surfaces machining framework. Both software and hardware integration to build functional modules of machining freeform and functional structure surface are under exploration.

Acknowledgement The authors would like to acknowledge the scholarship received from the UK's EPSRC Future Metrology Hub (Ref.: EP/P006930/1) on Mr Sumit Kumar's PhD study and UK's TURING Scholarship 2023 to undertake research at the Centre of Micro/Nano Manufacturing Technology (MNMT-Dublin), University College Dublin, Ireland. We also gratefully acknowledge Digital Surf for providing the educational license of MountainsMap® surface analysis software.

Availability of data and material The paper has no associated data.

Code availability The paper has no associated code.

Author contribution Sumit Kumar: Conceptualization, Methodology, Investigation, Resources, Writing—Original Draft, Writing—Review & Editing, Validation; Wenbin Zhong: Supervision, Resources, Writing—Review & Editing, Project administration; Guoyu Yu: Resources; Jufan Zhang: Resources; Wenhan Zeng: Supervision, Project administration, Funding acquisition, Resources; Xiangqian Jiang: Supervision, Funding acquisition, Project administration, Resources.

Funding The authors gratefully acknowledge the UK's Engineering and Physical Sciences Research Council (EPSRC) funding of Future Metrology Hub (Ref: EP/P006930/1), the UK's Science and Technology Facilities Council (STFC) Innovation Partnership Scheme (IPS) projects under grant agreement No. ST/V001280/1, and ST/W005263/1.

Declarations

Ethics approval and consent to participate Research participants were not subjected to harm in any ways whatsoever. The respect for the dignity of all the research participants had been prioritized, and full consent was obtained from the participants prior to the research study.

Consent for publication The authors consent to Springer the non-exclusive publication rights and warrant that their contribution is original and that they have full power to make this grant.

Competing interests The authors declare no competing interests.

References

1. Enoch JM (2007) Archeological optics: the very first known mirrors and lenses. J Mod Opt 54(9):1221–1239. https://doi.org/10.1080/09500340600855106
2. Anderson D, Burge J (2001) Optical fabrication. In: Malacara D (ed) Handbook of Optical Engineering, ch. 26, 1st edn. CRC Press, Boca Raton
3. Beaucamp A, Takizawa K, Han Y, Zhu W (2021) Reduction of mid-spatial frequency errors on aspheric and freeform optics by circular-random path polishing. Opt Express 29(19):29802–29812. https://doi.org/10.1364/OE.435945
4. Du C, Dai Y, Guan C, Hu HAO (2021) High efficiency removal of single point diamond turning marks on aluminum surface by combination of ion beam sputtering and smoothing polishing. Opt Express 29(3):3738–3753. https://doi.org/10.1364/OE.417537
5. Rolland JP, Thompson KP (2012) Freeform optics: evolution? No, revolution. SPIE news room 19:2012. https://doi.org/10.1117/2.1201207.004309
6. Fang FZ, Zhang XD, Weckenmann A, Zhang GX, Evans C (2013) Manufacturing and measurement of freeform optics. CIRP Annals 62(2):823–846. https://doi.org/10.1016/j.cirp.2013.05.003
7. Kumar S, Tong Z, Jiang X (2022) Advances in the design and manufacturing of novel freeform optics. Int J Extreme Manuf. https://doi.org/10.1088/2631-7990/ac7617
8. Pohl M, Kukso O, Boerret R, Rascher R (2020) Mid-spatial frequency error generation mechanisms and prevention strategies for the grinding process. J Eur Opt Soc-Rapid Publications 16(1):19. https://doi.org/10.1186/s41476-020-00140-9
9. Yu G, Reynolds C, Walker D, Fahnle O (2019) Study of footprint variations of CCP considering machine kinematics. EPJ Web Conf 215:05004. https://doi.org/10.1051/epjconf/201921505004

10. Coniglio J, Quattrociocchi N, Eisner M, Beagley S, Beck J, Brooks DR, Cox B, Perdue J, Nelson JD (2021) Smoothing mid-spatial frequency (MSF) errors on freeform optics with an algorithm-based robotic platform utilizing deflectometry input. In: SPIE Optifab, Rochester, New York, United States, 2021: Proc SPIE 11889. https://doi.org/10.1117/12.2602729
11. Aryan H, Suleski TJ (2019) Specification of optical surfaces with anisotropic mid-spatial frequency errors, In: Optical Design and Fabrication 2019 (Freeform, OFT), Washington, DC, United States, 2019: OSA Technical Digest, p OM4A.5. https://doi.org/10.1364/OFT.2019.OM4A.5
12. Dunn CR, Walker DD (2008) Pseudo-random tool paths for CNC sub-aperture polishing and other applications. Opt Express 16(23):18942–18949. https://doi.org/10.1364/OE.16.018942
13. Aryan H, Liang K, Alonso MA, Suleski TJ (2019) Predictive models for the Strehl ratio of diamond-machined optics. Appl Optics 58(12):3272–3276. https://doi.org/10.1364/AO.58.003272
14. Li L, Li X, Cheng Q, Li R, Deng W, Luo X, Zhang F, Xue D, Zhang X (2020) Optimized strategy to restrain the mid-spatial-frequency surface error in computer-controlled optical surfacing. Results Phys 19:103356. https://doi.org/10.1016/j.rinp.2020.103356
15. Harvey JE, Thompson AK (1995) Scattering effects from residual optical fabrication errors, In: International Conferences on Optical Fabrication and Testing, Tokyo, Japan. https://doi.org/10.1117/12.215588.
16. Noll RJ (1979) Effect of mid- and high-spatial frequencies on optical performance. Opt Eng 18(2):182137–182137. https://doi.org/10.1117/12.7972338
17. Huang Y, Fan B, Wan Y, Li S (2018) Improving the performance of single point diamond turning surface with ion beam figuring. Optik 172:540–544. https://doi.org/10.1016/j.ijleo.2018.07.039
18. Risse S, Scheiding S, Beier M, Gebhardt A, Damm C, Peschel T (2014) Ultra-precise manufacturing of aspherical and freeform mirrors for high resolution telescopes. In: Advances in optical and mechanical technologies for telescopes and instrumentation. Proc SPIE 9151, Montréal, Quebec, Canada. https://doi.org/10.1117/12.2056496
19. Khan GS, Gubarev M, Speegle C, Ramsey B (2010) Computer-controlled cylindrical polishing process for development of grazing incidence optics for hard X-ray region. In: SPIE Optics and Photonics Conference 2010. San Diego, CA, USA https://ntrs.nasa.gov/citations/20100036654
20. Khaghani A, Cheng K (2020) Investigation on multi-body dynamics based approach to the toolpath generation for ultraprecision machining of freeform surfaces. Proc Inst Mech Eng B J Eng Manuf 234(3):571–583. https://doi.org/10.1177/0954405419863961
21. Plummer WT, Baker JG, Van Tassell J (1999) Photographic optical systems with nonrotational aspheric surfaces. Appl Optics 38(16):3572–3592. https://doi.org/10.1364/AO.38.003572
22. Muslimov Eduard, Hugot Emmanuel, Jahn Wilfried, Vives Sebastien, Ferrari Marc, Chambion Bertrand, Henry David, Gaschet Christophe (2017) Combining freeform optics and curved detectors for wide field imaging: a polynomial approach over squared aperture. Opt Express 25(13):14598–14610. https://doi.org/10.1364/OE.25.014598. (**in English**)
23. Ye J, Chen L, Li X, Yuan Q, Gao Z (2017) Review of optical freeform surface representation technique and its application. Opt Eng 56(11):110901. https://doi.org/10.1117/1.OE.56.11.110901
24. Tong Z, Zhong W, S. To, Zeng W (2020) Fast-tool-servo micro-grooving freeform surfaces with embedded metrology. CIRP Annals 69(1):505–508. https://doi.org/10.1016/j.cirp.2020.04.111
25. Tobler WR (1970) A computer movie simulating urban growth in the Detroit Region. Econ Geogr 46:234–240. https://doi.org/10.2307/143141
26. Jiang X, Cooper P, Scott PJ (2011) "Freeform surface filtering using the diffusion equation," Proceedings: Mathematical. Phys Eng Sci 467(2127):841–859. http://www.jstor.org.libaccess.hud.ac.uk/stable/41059610
27. ISO, EN (1996) 3274: 1996/COR 1: 1998; Geometrical Product Specifications (GPS)—Surface Texture: Profile Method—Nominal Characteristics of Contact (Stylus) Instruments. ISO: Geneva, Switzerland.
28. Zeng W, Jiang X, Scott PJ (2011) Roundness filtration by using a robust regression filter. Meas Sci Technol 22(3):035108. https://doi.org/10.1088/0957-0233/22/3/035108
29. Zeng W, Jiang X, Scott PJ (2010) Fast algorithm of the robust Gaussian regression filter for areal surface analysis. Meas Sci Technol 21(5):055108. https://doi.org/10.1088/0957-0233/21/5/055108
30. ISO (2021) ISO, EN (2021) 25178-2:2021; Geometrical Product Specifications (GPS) — surface texture: areal — Part 2: Terms, Definitions and Surface Texture Parameters. International Standards Organization
31. ISO (2017) ISO, EN (2017) 10110-7:2017; Optics and Photonics—Preparation of Drawings for Optical Elements and Systems—Part 7: Surface Imperfections. International Standards Organization (ISO), Geneva, Switzerland